DEFENCE S&T TECHNICAL BULLETIN

VOL. 14 NUM. 1 YEAR 2021 ISSN 1985-6571

CONTENTS

Ministry of Defence Malaysia

SCIENCE & TECHNOLOGY RESEARCH INSTITUTE FOR DEFENCE (STRIDE)

MEASUREMENT OF OPTIMAL STRETCHABILITY GRAPHENE CONDUCTIVE INK PATTERN BY NUMERICAL ANALYSIS

Ameeruz Kamal Ab Wahid[1,2], Mohd Azli Salim[2,3*], Murni Ali[4], Nor Azmmi Masripan[2,3], Feng Dai[5] & Adzni Md. Saad[3]

[1]Jabatan Kejuruteraan Mekanikal, Politeknik Sultan Azlan Shah (PSAS), Malaysia
[2]Advanced Manufacturing Centre, Universiti Teknikal Malaysia Melaka (UTeM), Malaysia
[3]Fakulti Kejuruteraan Mekanikal, Universiti Teknikal Malaysia Melaka (UTeM), Malaysia
[4]NanoMalaysia Berhad, 157 Hampshire Place Office, Kuala Lumpur, Malaysia
[5]China Railway Eryuan Engineering Group Co., China

[*]Email: azli@utem.edu.my

ABSTRACT

This study determines the optimal stretchability performance of graphene conductive patterns by using maximum principal elastic strain and Von Mises stress analysis. It was performed by using experimental and finite element analysis (FEA) modelling approaches. The experimental work was initiated by obtaining the optimal formulation of the conductive ink based on the resistivity values and 20 wt.% of graphene nanoplatelets (GNP) was selected. Then, the Young's modulus and Hardness values for this formulation were determined to become the input for the FEA modelling. Six different types of pattern were developed for FEA analysis, which are the straight-line, sine wave, semi-circle, serpentine, zigzag and horseshoe as the straight-line pattern becomes the baseline. The sine wave pattern produced the best results as the percentage different with the baseline pattern in terms of maximum principal elastic strain and Von Mises stress were the largest with the value of 37 times lower. This is due to the fact that the sine wave has more edge and depicts the spring-like behaviour which produces better stretchability. The increased length of the pattern also contributes to stretchability performance. Furthermore, this study shows that the FEA approach can be utilised in investigating the stretchability performance of conductive ink.

Keywords: *Graphene conductive ink; stretchability; maximum principal elastic strain; Von Mises; ink pattern.*

1. INTRODUCTION

Stretchable and conductive materials have been widely used in electronic equipment and health care (Ha *et al.*, 2018). It is also expected to be widely used for electronic equipment in the future especially in automotive safety. Stretchable conductive ink (SCI) is one of the automotive safety applications of stretchable and conductive materials. Numerous forms of conductive inks with specific fillers such as polymers, carbon nanotubes, and metal nanoparticles or organic metal complexes for the creation of conductive patterns have been produced (Yang & Wang, 2016). Among these, graphene-based inks have been the most favoured metal inks and are under rapid development for flexible electronics applications. Because of the strong van der Waals forces between adjacent layers, the graphene sheets are inherently stacked together. Then, it is difficult to exfoliate and distribute graphite nanosheets evenly into a polymer matrix (Xue *et al.*, 2019).

Flexibility and expandability are the main features of the SCI while maintaining high conductivity levels. The layout of a standard driver health monitoring system is designed to continuously monitor parameters related to drivers, vehicles, and the environment by obtaining data from a variety of sensors and taken from the driver's body, interior, and exterior of the vehicle. Different types of drivers give different results due to the detection of mechanical pressure and strain, temperature variations, and bio-potential changes in the human body (Ha *et al.*, 2018).

A sine wave screen printed pattern using a stretchable conductive ink on a stretchable substrate is more stretchable than a similarly fabricated straight line pattern. Stretchability in the printed conductor context is defined as the percentage change in resistance of the printed conductor when exposed to induced uni-axial stress. The lower the change in resistance is better for the stretchability (Zhang *et al.*, 2018). The employment of wavy patterns is an intuitive mechanical technique to enhance the stretchability of stretchable electronics. The hypothesis is that the wavy or meandering patterns will behave like a spring coil, which will open up when they are stretched and should exhibit higher stretchability (Mohammed, 2017). It can be stretched with the same amount as a straight-line pattern but depicts a smaller increase in resistivity.

Hsu *et al.* (2010) published a paper describing the stretching behaviour of horseshoe-shaped wavy conductor copper lines which were created using a photolithographic process and covered on both sides within a Polydimethylsiloxane (PDMS) substrate. They have stretchability up to 100% before exhibiting electrical rupture. Jahanshahi *et al.* (2013) also discussed the horse-shoe patterns, which demonstrated that the meandering patterns with circular shapes exhibit a lower amount of plastic strain. The samples were prepared using a printed circuit board (PCB) approach and a thin film-based, polyimide supported approach. Both papers demonstrated that the horseshoe pattern exhibits lower stress than a straight-line and the highest stress concentration can be found in the crest of the horseshoe (Hsu *et al.*, 2010; Jahanshahi *et al.*, 2013).

The use of conductive nanomaterials for printed electronics must overcome two major challenges: first, similar to bulk metal, the printed patterns need high electrical conductivity and second, the nature of the substrate material is not affected (especially for plastic electronics) and needs to achieve high electrical conductivity under relatively light conditions (Kamyshny & Magdassi, 2019). Both of these challenges are important for conductive ink because the conductive nanomaterial content needs to be high. The higher its concentration in the ink, the better electrical conductivity which also needs flexible substrates compatibility and excellent bending stress tolerance (Yang & Wang, 2016).

Graphene has the greatest potential as high-performance absorption material due to its many attractive properties, including unique structure effects, high specific surface area, and high conductivity (Saad *et al.*, 2020). Graphene as a filler is capable of enhancing the performance, functionality as well as durability of many applications for the next generation of electronic devices, composite materials, and energy storage devices due to its outstanding electrical, mechanical, and thermal properties (Olabi *et al.*, 2021). The use of graphene as a filler element is because of its low cost and high conductivity, which is suitable for industrial-scale production. Most processes of graphene ink use organic solvents such as N-methyl-2-pyrrolidone (NMP) and Dimethylformamide (DMF), which are hazardous, low-concentration, and unsustainable which prohibits their usage in industrial production (Pan *et al.*, 2018). The use of GNP mixing with epoxy resin and hardener is sufficient to formulate a simple and low-cost high yield electrical conductive adhesives (ECA) route production process that is highly desirable for the practical application of graphene inks (Tran *et al.*, 2018).

The research work aimed to demonstrate the comparative difference in strain and stress caused by stretching the screen printed straight-line pattern (baseline) and a curving wave pattern. An experimental investigation was conducted to explore the resistivity of the conductive inks**.** By using experimental results as the input parameter for material properties in FEA modelling, the estimation of the maximum principal elastic strain can be calculated. The differential in strain and stress during stretching could also be optimised by determining the fatigue in different pattern lines. It can be estimated using the maximum principal elastic strain and equivalent stress (Von Mises stress) obtained through FEA modelling. Von Mises stresses were used to evaluate the stress distribution in the conductive ink patterns because a higher Von Mises stress provides a strong indication of a greater possibility of failure (Spazzin *et al.*, 2013). After achieving the stated aim above, an attempt was also made to determine the best-printed conductor pattern with the most optimal stretchability by using maximum principal elastic strain and Von Mises stress obtained from FEA modelling.

2. METHODOLOGY

2.1 ECA Sample Preparation

The epoxy / graphene ink formulations were prepared using a planetary centrifugal mixer. The curing process or the annealing of ECA after the mixing process used the high temperature oven. The new formulation of stretchable conductive ink was characterised in terms of electrical and mechanical behaviours. The formulation of graphene with different filler loadings was characterised to determine and select the suitable ECA, which can satisfy the functionality. The ECA was fabricated with the most basic shape or pattern and tested with electrical and mechanical behaviours (Strehmel *et al*., 2015). In this research, there were three main materials used to formulate the conductive ink. The main materials for ECA formulation are shown in Table 1.

Table 1: Main materials of conductive inks.

Materials	**Descriptions**
Graphene nanoplatelets (GNP) powder	As filler elements
Araldite M or CY 212 (epoxy resin)	As binder elements (to bind the particles)
Huntsman polytheramine D230 (hardener)	To harden or dry the mixtures

GNP as filler element, Araldite® as epoxy resin, and Huntsman polytheramine as hardener were used as the main material for this research which received without further modification. All the raw materials (GNP, epoxy, and hardener) were precisely weighed using an analytical balance. The properties of GNP available from the product datasheet were presented in Table 2.

Table 2: Properties of GNP.

Specification	
Form	**Powder**
Surface area	50-80 m^2/g
Average flake thickness	15 nm
Average particle size	5 µm
Density	0.03 – 0.1 g/cm^3

For the filler loading experiment, the change in the percentage of graphene mass mixed with the epoxy as a binder was to determine the resistance of the ECA. All samples were tested according to each applicable test to evaluate certain characterisations and the average data of these samples become the final result. The conductive ink typically includes between about 40-60 % of conductive particles and between about 30-50 % of binder. The stretchable conductive ink patterns may be stretched more than twice of their length without breaking or rupturing (Longinotti & Aliverti, 2017). The formulation contained 0.5 g of resin and hardener was prepared using a planetary centrifugal mixer. To obtain the filler percentage, the filler domain was divided into 5 samples starting with 10 wt.% with each sample interval representing 5 wt.% and followed by mixing with 70-90 wt.% of binder (epoxy) and hardener (30% of epoxy weight) respectively.

Table 3 tabulates the formulation of the materials in the development of the ECAs, in which the GNP was varied, between 10 wt.% to 30 wt.%. The hardener (30% of epoxy weight) as a curing agent was mixed with graphene and epoxy to obtain the total amount of formulations, followed by a mixing process with all involving materials using a planetary centrifugal mixer at 2000 rpm for three minutes. The planetary centrifugal mixing was used to achieve a uniform dispersion and to enable high precision in the desecration of high-viscosity adhesives and materials whose viscosities are increased by added fillers. After the mixing process, the formulation was done by the doctor blading method on the glass slide substrate before the curing process. Figure 1 shows the thickness (t_s), width (w), and length (l) of the conductive inks with the values of 0.1, 3.0 and 25.4 mm respectively.

Table 3: Formulation of the materials in the development of the ECAs.

Sample	GNP		Epoxy		Hardener (g)
	(wt.%)	(g)	(wt.%)	(g)	
S10	10	0.050	90	0.450	0.135
S15	15	0.075	85	0.425	0.128
S20	20	0.100	80	0.400	0.120
S25	25	0.125	75	0.375	0.113
S30	30	0.150	70	0.350	0.105

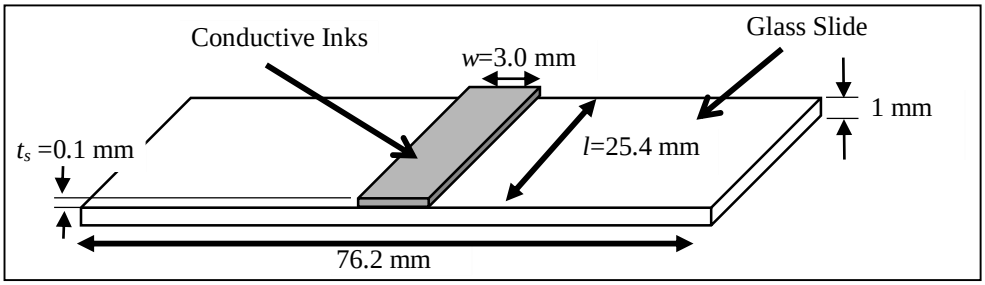

Figure 1: Pattern thick layer dimension of ECA on the glass slide.

All formulations were cured in a high temperature oven at 150 °C for 30 min. Higher temperatures or longer annealing times are required in order to increase conductivity (Karagiannidis *et al.*, 2017). But there is a risk of using higher temperatures and longer annealing times e.g. higher than 300 °C with sintering time over 3 hours are not practical to be implemented on flexible substrates (Yang & Wang, 2016). After the curing process, all specimens were normalised at room temperature for about 24 h. Figure 2 shows the specimen of 20 wt.% (S20) on a glass slide with three minutes of mixing times.

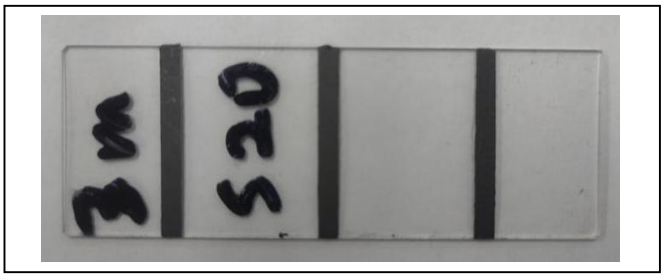

Figure 2: Specimen with three layers on the glass slide.

2.2 ECA Experimental

After all the samples had been prepared, each of these samples underwent an electrical characterisation analysis to obtain the sheet resistance values by using the In-Line Four-Point Probe. The input was ranged between 10 nA to 100 mA at three different locations per stripes, which equals to nine data per sample (refers to Figure 3 for the sample marking points). Then, the data was analysed to get the volume of resistivity for all the samples and the average of the volume of resistivity and standard deviation values were determined. All samples were tested according to each applicable test standard to evaluate certain characterisation in which the average data of these samples become the final result.

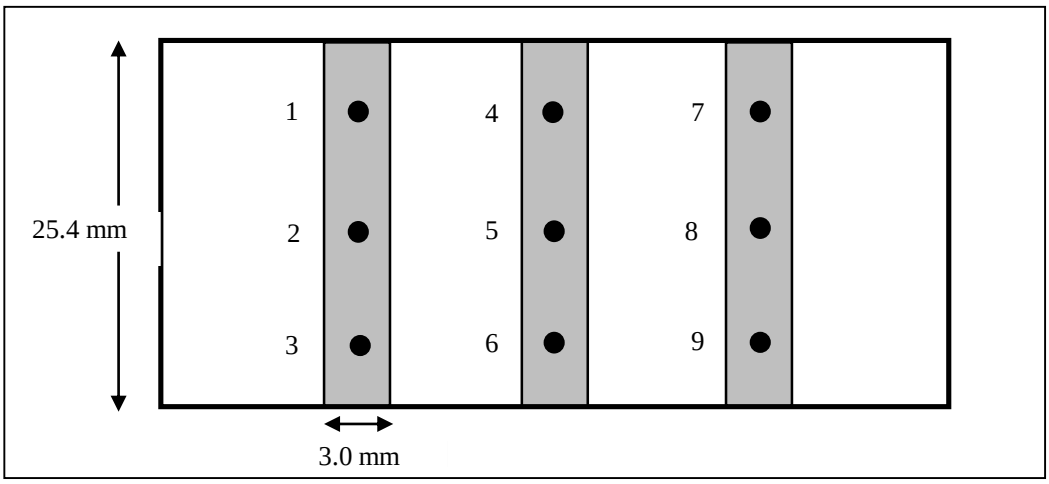

Figure 3: Schematic of printed conductive ink on a glass slide with 9 marking points.

The measurement of resistivity (average sheet resistance, the average volume of resistivity and, standard deviation values) of the filler loading percentage measurements are presented in Table 4. S10 and S15 samples represent GNP of 10 wt.% and 15 wt.% respectively showed very high values of sheet resistance, volume of resistivity, and standard deviation. The loss modulus was higher for both 10 wt.% and 15 wt.% of graphene than the storage modulus throughout the range of the measured stresses, indicating that these formulations displayed liquid-like behaviour. This makes the ratio of 10 wt.% and 15 wt.% are not suitable for use in the circuit because of their high resistance value. Samples S20, S25, and S30 did not show a significant difference between all the results because the use of binder content was less for the three samples. It makes the samples possess less liquid behaviour after the curing process. Salim *et al*. (2020) stated that the higher the vehicle (binder polymer and solvents) content of the ink, the more uneven the printed ink layer surface when produced using the offset lithography method.

Table 4: Measurement of resistivity of the test samples.

Sample	Sheet Resistance, Average (R/sq)	Volume of Resistivity, Average (Ω.cm)	Standard Deviation (Ω.cm)
S10	55.5161×10^6	330.7764×10^3	296.8148×10^3
S15	1.1436×10^6	6.8139×10^3	1.5557×10^3
S20	4.1799×10^3	24.9046	4.4328
S25	3.9784×10^3	23.7043	3.5152
S30	2.1655×10^3	12.9024	3.2456

Figure 4 illustrates a very high volume of resistivity for a sample of 10 wt.% with the value of 330.7764 x 10^3 Ω.cm as compared to other samples. This makes the sample of 10 wt.% was rejected. There was a significant difference in the average volume of resistivity between 15 wt.% with the value of 6.81396 x 10^3 Ω.cm, and 20 wt.% with the value of 24.9046 Ω.cm. This makes the GNP at 15 wt.% was also rejected because of high resistance recorded. Samples 20, 25 and 30 wt.% did not show significant differences in terms of the average volume of resistivity. This indicates that the resistance found in samples 20, 25 and 30 wt.% did not significantly affect the flow rate in the circuit.

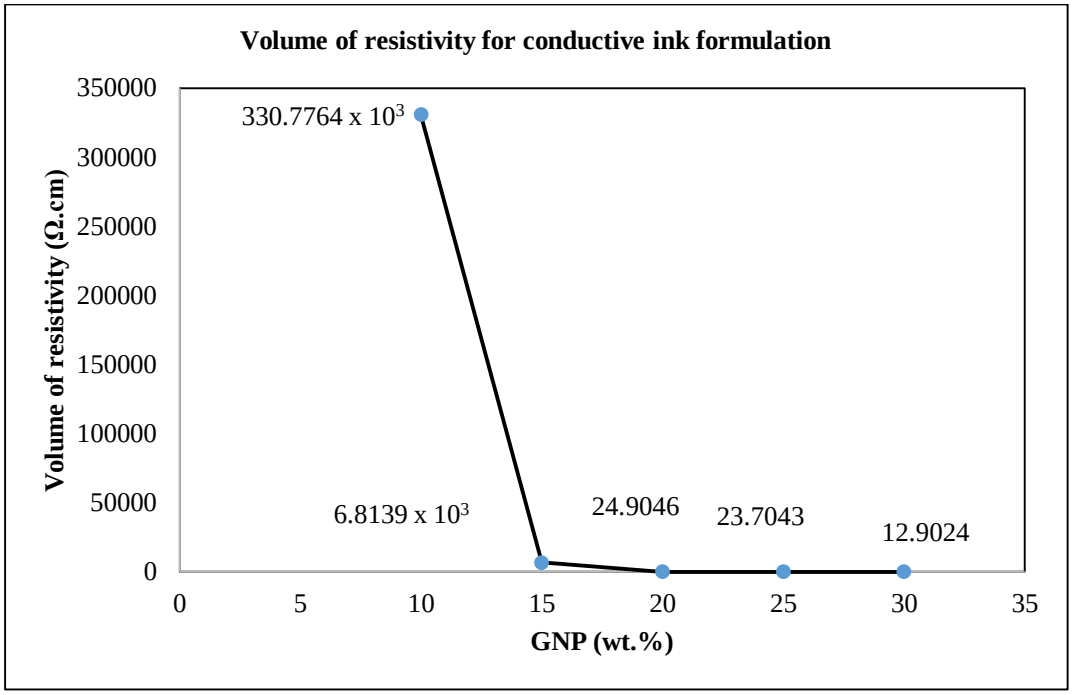

Figure 4: Volume of resistivity (Ω/cm) on conductive ink formulation.

2.3 Mechanical Characterisation Analysis

From the data in the filler loading experiment, sample S20 was selected for mechanical characterisation analysis because it is more economical in terms of material usage. Most studies on graphene and its application are focused on the reduction of graphene materials since graphene can be produced cost-effectively on an industrially accessible scale, and the graphene functional groups enable its hydrophilicity and processability of formulations (Tran *et al.*, 2018). For this experiment, the main focus is on the mechanical properties, which can determine the strength of the material. The hardness of ECAs samples was tested using a nano-indentation machine. In determining the suitable maximum force for this experiment, several force values were tested by using the selected sample from the filler loading experiment. Nano-indentation depth was carefully adjusted to avoid cracking and rupture of the formulation and consequently loss of protective effect. Table 5 shows the Young's Modulus and hardness values with different maximum forces.

Table 5: Young's Modulus and hardness value for determining suitable maximum force.

Sample	Maximum Force (mN)	Maximum Depth (μm)	Young's Modulus, E (GPa)	Hardness (MPa)
S20	50	2.8261	10.27	28.932
	60	3.0399	9.569	30.772
	80	4.5182	7.621	17.555
	100	4.2886	8.698	25.19
	150	5.5434	15.49	20.318
	175	12.4837	1.912	4.956

From the same table, 150 mN was a suitable maximum force to perform this experiment because the value of Young's Modulus was the highest as compared to other maximum forces. The maximum load was measured as a function of penetration depth of the indenter into the surface (Batakliev *et al.*, 2018), and may penetrate too deep if the load is too high, but a major concern when measuring thin films because the results would then be influenced by the substrate's properties. On the other hand, if the load

is too low, then the roughness of the specimen surface will affect the results. The maximum force of 175 mN as compared to others has a maximum depth that is too high. This allows the depth of penetration to get too deep and results in a sharp decrease in the Young's Modulus and hardness values. The Young's Modulus can determine the physical properties of the formulation by allowing the bending or stretching of conductive ink circuits. The Young's modulus values from this experiment then were used as the input parameter in FEA of graphene formulation.

2.4 Finite Element Pre-Processing Analysis

The numerical workbench software was used for the FEA of the Knuckle joint. At first, the Knuckle Joint was designed in design **s**oftware, CATIA and then the file was saved as IGES format and imported into the workbench software. The next step was to mesh the model with fine mesh option and a reasonable time was required for the computational process as shown in Figure 5. The finite element was generated using the element size of 1.9 x 10^{-4} mm which makes it from 6915 to 18148 elements depending on the shape of the patterns.

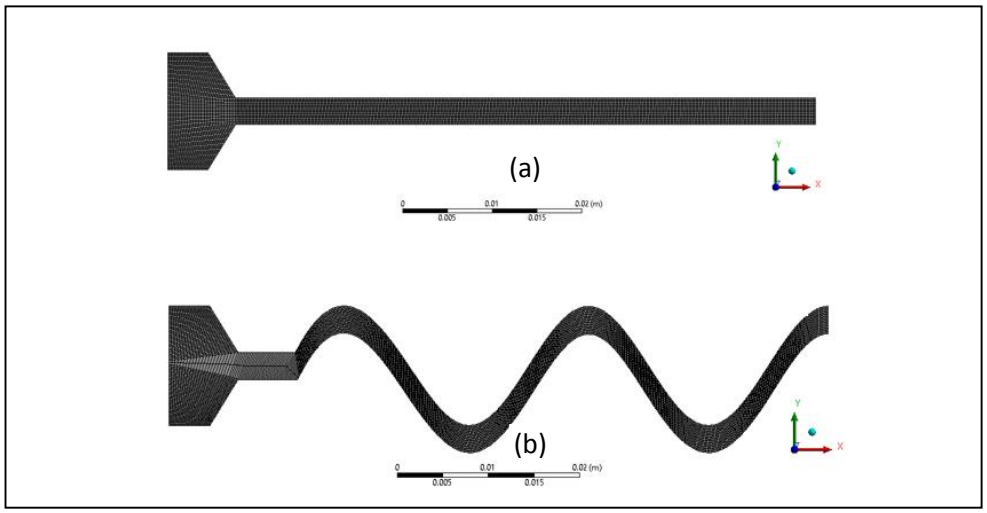

Figure 5: Mesh model of samples. (a) Straight-line pattern. (b) Sine wave pattern

2.5 FEA

The FEA of ink stresses on a wavy pattern and a straight-line screen-printed pattern was analysed using ANSYS software to simulate strain and stress behaviour of the circuit under mechanical loading. The ink was modelled as a layered structure to simulate the screen-printed process. The objective of the analysis was to assess the influence of the six different printed shapes, straight-line (baseline), sine wave, semi-circle, serpentine, zigzag and horseshoe on the resultant stresses on the printed pattern. The shapes were printed on the same substrate using similar printing and curing processes. This analysis was designed to estimate which shape would exhibit lower stress by its percentage value. The material properties obtained from the previous experimental results and ink supplier were shown in Table 6. Then, the numerical results were compared with the experimental results.

Table 6: Material properties used for simulation analysis.

Materials	Properties				
	Young's modulus (Pa)	Poisson's ratio	Density (kg/m^3)	Thermal conductivity (W/m °K)	Resistivity (Ω.m)
Graphene	15.49 x 10^9	0.149	2200	5300	0.249

The FEA model was developed with 0.1 mm ink thickness for all patterns. Because of symmetrical

geometry along the X direction, a half model was deployed. According to Mohammed (2017), the stretch reliability test requires a few percent stretch, e.g. 10% or 20% to determine the estimated lifetime under a particular strain of the stretchable conductors. The 20% of elongation stress was deployed uni-axially along the X-axis as shown in Figure 6.

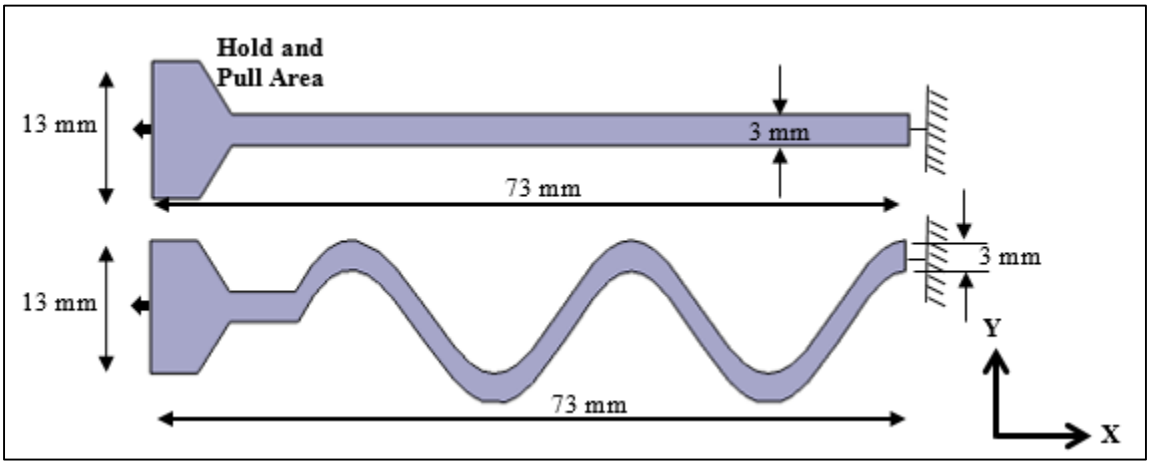

Figure 6: FEA symmetrical half model.

3. RESULTS AND DISCUSSIONS

3.1 Comparison between Straight Line (Baseline) and Other Wavy Patterns

Table 7 shows the percentage difference between straight line (baseline) and other patterns on the maximum principal elastic strain and Von Mises stress. Percentage difference is used to evaluate the difference between other patterns with the straight line (baseline) pattern. The negative value generated indicates the lack of other pattern values against the straight line (baseline) pattern. The comparison of the percentage to the straight line (baseline) shows that the sine wave is the lowest and is followed by horseshoe, zigzag, semi-circle, and serpentine. The percentage difference value of sine wave is -189.57% for maximum principal elastic strain and -187.62% for Von Mises stress. It can also be stated that the sine wave percentage value is 189.57% lower at maximum principal elastic strain and 187.62% lower at Von Mises stress than a straight line (baseline). This can be seen through the observation in Figures 7 and 8, where the curves found in the wavy pattern greatly reduce the value of strain and stress on the pattern. All percentage differences are solved using the following equation:

$$\%\ \ Difference = \frac{V_1 - V_2}{\left(\frac{V_1 + V_2}{2}\right)} \times 100 \tag{1}$$

where:

V_1 = Other patterns (maximum principal elastic strain or Von Mises stress) value
V_2 = Straight line (maximum principal elastic strain or Von Mises stress) value

Figures 7 and 8 show the comparisons of the maximum principal elastic strain and Von Misses stress for six patterns. It can be seen that the maximum principal elastic strain and equivalent stress (Von Mises stress) behaviours are different for all the patterns. Based on the result, the maximum principal elastic strain and equivalent stress are lower on a more curving pattern because the curving pattern has the edge. The type (b) pattern in Figures 7 and 8 attain the smallest amount of maximum principal elastic strain and Von Mises stress among all the six types because of the sine wave pattern depicting the spring coil behaviour. The length of the pattern also gives an effect to the stress and strain value. If the length increases, the Von Mises stress value is reduced below 1000 MPa, thus improving the mechanical reliability of the device (Zulkefli *et al.*, 2017). However, type (a) attains the highest value of stress among all the patterns because it does not possess high stretchability behaviour.

Table 7: FEA results summary for the half model.

Component	Type	Pattern	Maximum Principal Elastic Strain	% Difference to Baseline (%)	Von Misses Stress (MPa)	% Difference to Baseline (%)
Ink	a	Straight Line (Baseline)	0.5452	0	8060	0
	b	Sine Wave	0.0146	-189.57	257.34	-187.62
	c	Semi-Circle	0.0839	-146.65	1300.1	-144.44
	d	Serpentine	0.1777	-101.67	2552.1	-103.80
	e	Zigzag	0.0263	-181.59	396.21	-181.26
	f	Horseshoe	0.0193	-186.32	298.55	-185.71

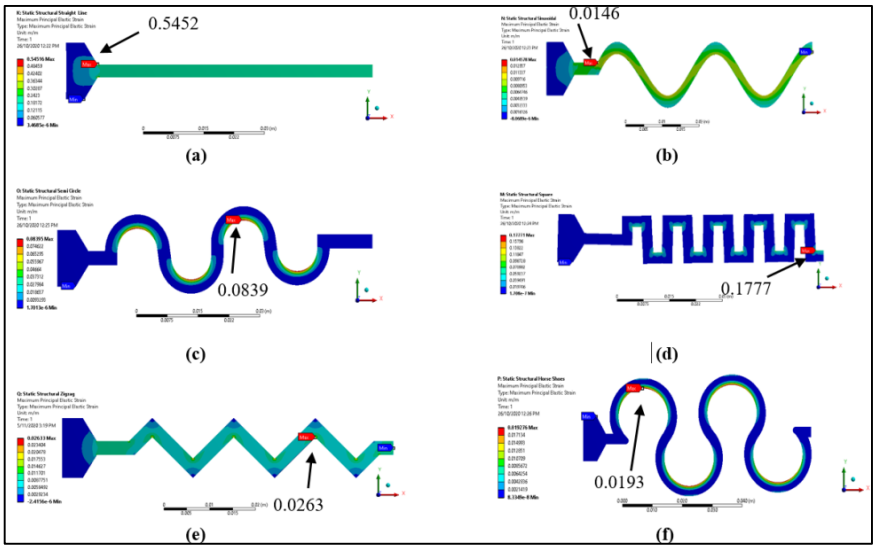

Figure 7: Maximum Principal Elastic Strain. (a) Straight line trace; (b) Sine wave trace; (c) Semi-circle trace; (d) Serpentine trace; (e) Zigzag trace; (f) Horseshoe trace.

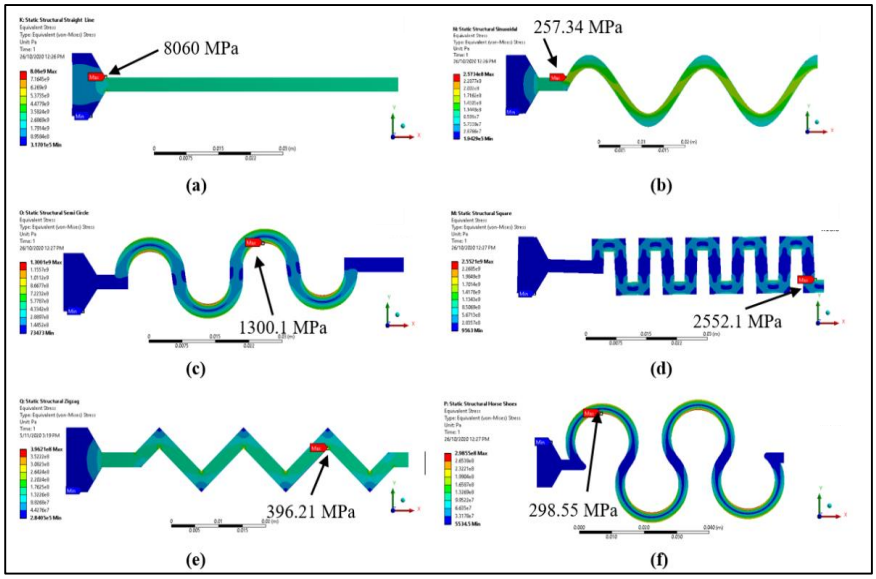

Figure 8: Von Mises Stress. (a) Straight line trace; (b) Sine wave trace; (c) Semi-circle trace; (d) Serpentine trace; (e) Zigzag trace; (f) Horseshoe trace.

From the FEA performed, the maximum principal elastic strain for each of the six patterns was calculated by assuming that the lowest maximum principal elastic strain would offer the best stretchability performance. From the observation in Figure 7, the straight-line pattern can withstand more stress than the other wavy patterns. By using the maximum principal elastic strain, the sine wave pattern has the largest percentage difference when comparing to the straight-line (baseline) pattern, which is about 37 times less strain. The nearest values of maximum principal elastic strain and equivalent stress (Von Mises) to the straight-line pattern are the serpentine pattern, which is three times lower with the percentage values of -101.67% and -103.8% respectively. Based on the results in Figures 7 and 8, the correlation between maximum principal elastic strain and Von Mises stress to the percentage difference in Table 7 between baseline and other patterns for both analyses are almost the same. This indicates that the 20% strain and stress exposure on both analyses have similar effects on the conductive ink behaviour between the straight-line (baseline) pattern and other curving patterns.

The FEA results demonstrate that the sine wave pattern has better stretchability as compared to a straight-line pattern. The sine wave pattern behaves like a coil and opens up under stretch whereas the straight line does not have that capability. The results are similar to what is available in the literature (Hsu *et al*., 2010) for a horseshoe type pattern that was not screen printed. The FEA estimates the stretchability of the straight-line pattern to be 37 times worse than the sine wave pattern after 20% of strain exposure. This FEA value assumes an ideal situation with no delamination between the ink and the substrate, no stress cycling, and no variations during the manufacturing process. Nevertheless, the FEA model does validate the assumption and the FEA results that a sine wave pattern tends to behave like a spring coil and exhibits less strain versus a straight-line pattern.

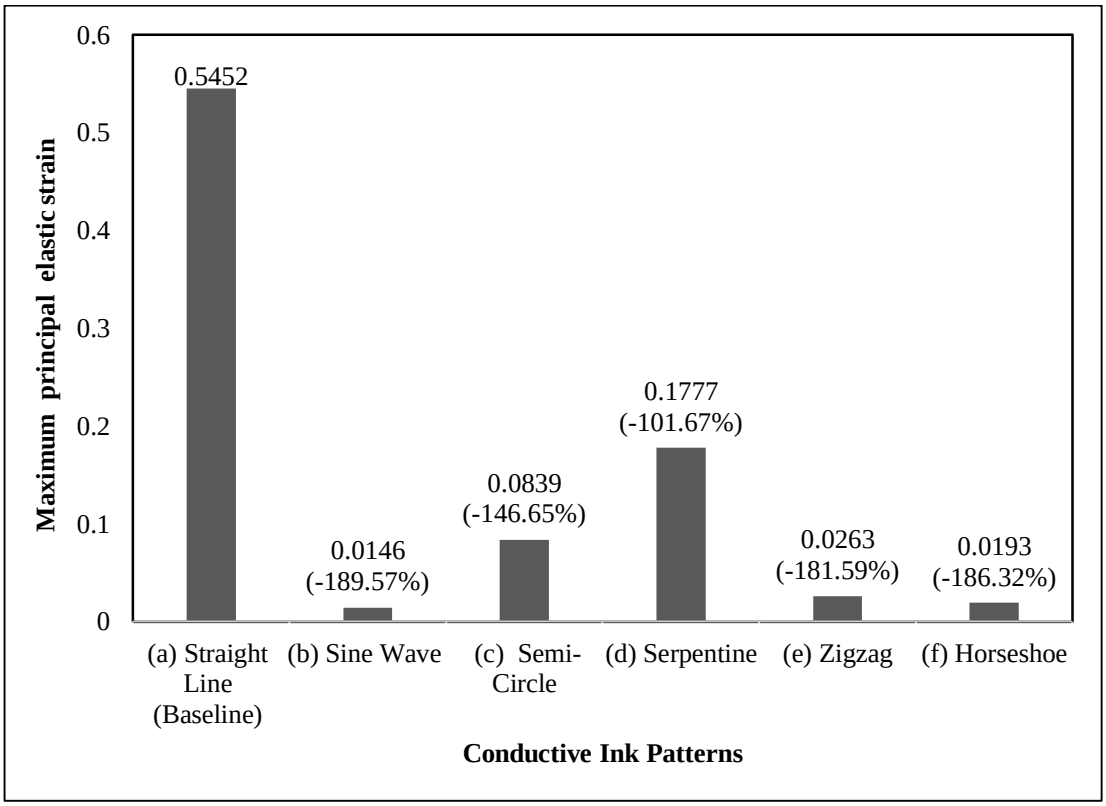

Figure 9: Percentage difference between the straight line (baseline) pattern and other wavy patterns using maximum principal elastic strain.

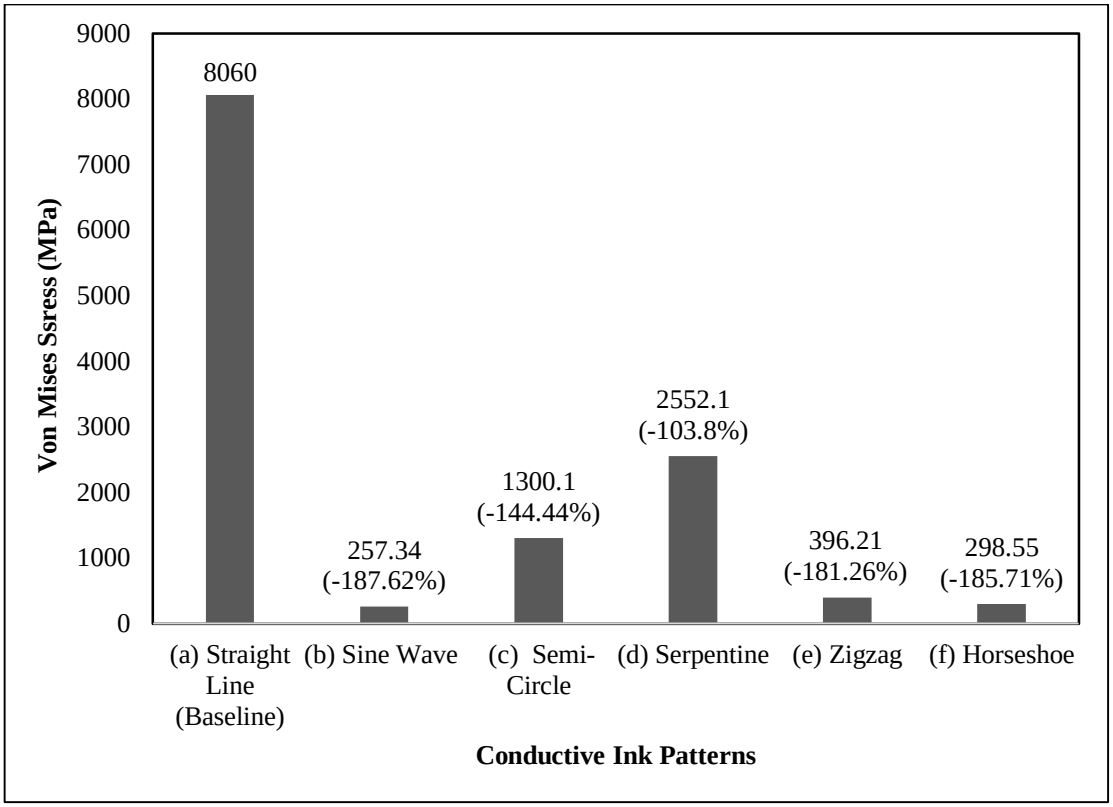

Figure 10: Percentage difference between the straight line (baseline) pattern and other wavy patterns using Von Mises stress.

4. CONCLUSION

The study was carried out successfully in demonstrating the optimal stretchability performance of graphene conductive patterns by using maximum principal elastic strain and Von Mises stress analysis. In terms of maximum principal elastic strain and Von Mises stress, the sine wave pattern provided the best results as the percentage difference from the baseline pattern was the highest with a value of 37 times lower. It is because the sine wave has more edge and depicts the spring-like behaviour. The increased length of the pattern also contributes to stretchability performance. The findings also demonstrated that the optimal screen-printed pattern for stretchability could be designed by using FEA modelling and the maximum principal elastic strain could be used to estimate the increase in the change of resistance during stretching.

ACKNOWLEDGEMENT

Special thanks to the Advanced Manufacturing Centre (AMC) and Fakulti Kejuruteraan Mekanikal (FKM), Universiti Teknikal Malaysia Melaka (UTeM) for providing the laboratory facilities.

REFERENCES

Batakliev, T., Georgiev, V., Ivanov, E., Kotsilkova, R., Di Maio, R., Silvestre, C. & Cimmino, S. (2019). Nanoindentation analysis of 3D printed poly (lactic acid) -based composites reinforced with graphene and multiwall carbon nanotubes. *J. Poly. Sci.*, **136**: 47260.

Ha, M., Lim, S. & Ko, H. (2018). Wearable and flexible sensors for user-interactive health-monitoring devices. *J. Mater. Chem. B*, **6**: 4043-4064.

Hsu, Y.Y., Gonzalez, M., Bossuyt, F., Axisa, F., Vanfleteren, J. & De Wolf, I. (2010). The effect of

pitch on deformation behaviour and the stretching-induced failure of a polymer-encapsulated stretchable circuit. *J. Micromech. Microeng.*, **20**: 075036.

Jahanshahi, A., Gonzalez, M., van den Brand, J., Bossuyt, F., Vervust, T., Verplancke, R. & De Baets, J. (2013). Stretchable circuits with horseshoe shaped conductors embedded in elastic polymers. *Jpn. J. Appl. Phys.*, **52**: 05DA18.

Kamyshny, A. & Magdassi, S. (2019). Conductive nanomaterials for 2D and 3D printed flexible electronics. *Chem. Soc. Rev.*, **48**: 1712-1740.

Karagiannidis, P.G., Hodge, S.A., Lombardi, L., Tomarchio, F., Decorde, N., Milana, S. & Ferrari, A.C. (2017). Microfluidization of graphite and formulation of graphene-based conductive inks. *ACS Nano.*, **11:** 2742-2755.

Longinotti-buitoni, G. & Aliverti, A. (2017). *U.S. Patent No. 9,817,440: Garments Having Stretchable and Conductive Ink.* U.S. Patent and Trademark Office, Washington, DC.

Mohammed, A.A. (2017). *Development of a New Stretchable and Screen Printable Conductive Ink*, Doctoral dissertation, University of Maryland, Maryland.

Olabi, A.G., Abdelkareem, M.A., Wilberforce, T. & Sayed, E.T. (2021). Application of graphene in energy storage device–A review. *Renew. Sust. Energ. Rev.*, **135**: 110026.

Pan, K., Fan, Y., Leng, T., Li, J., Xin, Z., Zhang, J. & Hu, Z. (2018). Sustainable production of highly conductive multilayer graphene ink for wireless connectivity and IoT applications. *Nat Commun*, **9**: 1-10

Saad, H., Salim, M. A., Masripan, N. A., Saad, A. M., & Dai, F. (2020). Nanoscale graphene nanoparticles conductive ink mechanical performance based on nanoindentation analysis. *Int. J.Nanoelectr. Mater.*, **13**: 439-448

Salim, M.A., Dai, F., Saad, A.M., Masripan, N.A., Dmitriev, A. N., Naroh, A. & Akop, M.Z. (2020). Prediction effects on internal resonance wave of metallic conductive ink in rotational motion behaviour *Int. J.Nanoelectr. Mater.*, **13**: 295-304

Shen, C. & Oyadiji, S.O. (2020). The processing and analysis of graphene and the strength enhancement effect of graphene-based filler materials: A review. *Mater. Today Phy.*, **15**: 100257.

Spazzin, A.O., Costa, A.R., Correr, A.B., Consani, R.L.X., Correr-Sobrinho, L. & dos Santos, M.B.F. (2013). Effect of bar cross-section geometry on stress distribution in overdenture-retaining system simulating horizontal misfit and bone loss. *J. Biomech.*, **46**: 2039-2044.

Strehmel, V., Berdzinski, S., Ehrentraut, L., Faßbender, C., Horst, J., Leeb, E. & Wenda, A. (2015). Application of ionic liquids in synthesis of polymeric binders for coatings. *Prog Org Coat*, **89**: 297-313.

Tran, T.S., Dutta, N.K. & Choudhury, N.R. (2018). Graphene inks for printed flexible electronics: graphene dispersions, ink formulations, printing techniques and applications. *Adv Colloid Interfac*, **261**: 41-61.

Yang, W. & Wang, C. (2016). Graphene and the related conductive inks for flexible electronics. *J Mater Chem C*, **4**: 7193-7207.

Young, R. J., Liu, M., Kinloch, I. A., Li, S., Zhao, X., Vallés, C. & Papageorgiou, D.G. (2018). The mechanics of reinforcement of polymers by graphene nanoplatelets. *Compos. Sci. Technol.*, **154**: 110-116.

Yu, H., Fang, D., Dirican, M., Wang, R., Tian, Y., Chen, L. & Zhang, X. (2019). Binding conductive ink initiatively and strongly: transparent and thermally stable cellulose nanopaper as a promising substrate for flexible electronics. *ACS Appl. Mater. Inter.*, **11**: 20281-20290.

Zhang, B., Lei, J., Qi, D., Liu, Z., Wang, Y., Xiao, G. & Chen, X. (2018). Stretchable conductive fibers based on a cracking control strategy for wearable electronics. *Adv. Funct. Mater.*, **28:** 1801683.

Zulkefli, M.A., Mohamed, M.A., Siow, K.S., Majlis, B.Y., Kulothungan, J., Muruganathan, M. & Mizuta, H. (2018). Stress analysis of perforated graphene nano-electro-mechanical (NEM) contact switches by 3D finite element simulation. *Micrisyst. Technol.*, **24**: 1179-1187.